


Article

Development and Characterization of Anticorrosion and Antifriction Properties for High Performance Polyurethane/Graphene Composite Coatings

Pei-Ying Tsai, Tzu-En Chen and Yueh-Lien Lee * 

Department of Engineering Science and Ocean Engineering, National Taiwan University, Taipei 10617, Taiwan; r04525074@ntu.edu.tw (P.-Y.T.); b03505026@ntu.edu.tw (T.-E.C.)

* Correspondence: yuehlien@ntu.edu.tw; Tel.: 886-2-33665740; Fax: 886-2-23929885

Received: 13 June 2018; Accepted: 13 July 2018; Published: 16 July 2018



Abstract: This work contributes to the development and characterization of the corrosion resistance and antifriction properties of high performance polyurethane (PU)/graphene (Gr) composite coating. In this study, PU composite coatings containing 0, 2, 4 and 8 wt.% of Gr were prepared and evaluated using various corrosion and mechanical tests, namely electrochemical impedance spectroscopy, salt spray tests, cross-cut tape tests and dynamic mechanical analysis. Antifriction properties of the coatings were evaluated using a tribometer with a ball-on-disc mode at room temperature. The corrosion resistance and adhesion property of the PU coatings were found to be enhanced by adding 4 and 8 wt.% of Gr. The coefficient of friction revealed that the antifriction properties of the PU/Gr composite coatings were 61% lower than those of the conventional coating when the Gr content was increased to 8 wt.%.

Keywords: polyurethane coating; graphene; corrosion; EIS; salt spray test; coefficient of friction

1. Introduction

Metallic substrates are susceptible to corrosion attacks in natural environments. Therefore, many corrosion protection treatments, such as electroplating, anodization, hot-dip galvanization, conversion coatings, corrosion inhibitors, barrier coatings and cathodic protection have been used to protect metallic substrates for many years. Among these treatments, organic coating is one of the easiest and cheapest ways to prevent corrosion. Organic coatings primarily serve as a physical barrier to protect a metal substrate from the electrochemical charge that comes from corrosive environments. However, organic coatings are not perfect barriers and are permeable to corrosive substances, such as Cl^- , O_2 and H_2O . The presence of water molecules at the coating–substrate interface may trigger electrochemical corrosion of a metal under the coating, leading to a decrease in adhesion strength and coating delamination. The barrier performance and permeability of organic coatings can be improved by the incorporation of inorganic fillers [1–15]. For instance, Dhoke and co-workers [1] found that the addition of nano-ZnO on the alkyd-based waterborne coating can enhance the density of the coatings thereby reducing the transport paths for the corrosive electrolyte to pass through the coating system and hence reducing the corrosion process. Shi et al. [2] investigated the effect of SiO_2 , Zn, Fe_2O_3 and halloysite clay nanoparticles' addition on the anticorrosion of epoxy coating. They showed that the incorporation of a small number of nanoparticles—especially Fe_2O_3 and halloysite clay—into the epoxy coating can enhance the corrosion resistance of the epoxy-coated steel. In recent years, it was reported that carbon derivatives, such as carbon nanotubes (CNTs) [16–18], graphene (Gr) and graphene oxide (GO) [19–31] can be used as anti-corrosion additives to organic coatings. Gr has attracted considerable attention owing to its extraordinary electrical and physical properties, especially its impermeable

nature [32–34]. There are a number of studies showing that adding Gr and its derivatives to a polymer coating can enhance the corrosion performance of the coating [19–31]. Yu et al. [19] reported that the corrosion protection efficiency increased from 37.90% to 99.53% with the incorporation of 2 wt.% modified GO in the polystyrene polymer matrix. Hayatgheib et al. [23] ascertained that incorporation of GO-PANI nanosheets into the epoxy matrix significantly enhanced the barrier performance and ionic resistance of epoxy coating. They also proposed that PANI nanofibers can enhance the epoxy coating ionic resistance through providing positive surface charge on the GO sheets and retarding the hydrated Na^+ cations migration to the cathodic regions. By using electrochemical impedance spectroscopy (EIS), potentiodynamic polarization curve and the salt spray test (SST), Liu et al. [24] found that the addition of Gr to epoxy resin effectively inhibited corrosion; they indicated that 0.5 wt.% of Gr provided the best corrosion resistance and the impedance value of the coating decreased slightly due to aggregation when 1 wt.% of Gr was added. Li et al. [25] found that the anticorrosion properties of polyurethane (PU) were enhanced by the addition of 0.2 wt.% of reduced graphene oxide (RGO).

Many mechanical properties of polymer materials, such as mechanical strength [35,36], tribological performance [37–42], thermal stability [19] and electrical conductivity [43,44], can be improved remarkably by incorporating carbon derivatives into polymers. In particular, the antifriction performance of polymer coatings is of practical importance because these coatings are susceptible to damage through scratching and abrasive wear under outdoor service conditions, leading to the loss of mechanical strength. The addition of high-performance nanofillers, such as ceramic particles into polymer coatings, is effective in enhancing their antifriction properties. Notably, recent investigations have revealed the significant potential of Gr and its derivatives for producing polymer composite coatings with high antifriction properties [38–42]. For instance, Mo et al. [38] investigated the tribological performance of PU composite coatings reinforced with functionalized Gr (FG) and Gr oxide (FGO) and found that FG and FGO enhanced the antifriction property of PU composite coatings owing to their lubricating effects. Moreover, they pointed out that the optimized additive range was from 0.25 to 0.5 wt.%. Liu et al. [39] evaluated the tribological resistance of an epoxy coating reinforced with functionalized fullerene C60 and Gr. They reported that the wear traces of the composite coating decreased with increases in the contents of functionalized fullerene C60 and functionalized Gr. However, the tribological resistance of the coating decreased with an increase in the contents to 0.5 wt.%. Chen et al. [40] successfully exfoliated Gr with a few atomic layers in an organic solvent by using P2BA as a dispersant. They found that embedding a small percentage of these well-dispersed Gr nanosheets ($\text{P2BA}_{0.5\%}\text{-Gr}_{0.5\%}$) in epoxy coating can remarkably improve the antifriction properties of the coating. Bandeira et al. [41] reported the antifriction property of a self-lubricating epoxy-PTEE coating modified with oxidized Gr nanoplatelets (GNPox). Their results proved that the incorporation of GNPox as a sole modifier into the base epoxy coating reduces the coefficient of friction (COF) of noise under both test regimes. Therefore, Gr can play an essential role in improving the anticorrosion and antifriction properties of polymer coatings. Although a few studies have reported that the anticorrosion and antifriction properties of polymer coatings can be simultaneously altered using Gr additives [38–40], the Gr contents employed in those works were relatively low. Moreover, the COF of composite coatings used in those studies increased rapidly to a higher value (over 0.5) after a short sliding distance and the impedance modulus of the composite coatings at the lowest frequency in the Bode plot decreased with the passage of measurement time under immersion in 3.5 wt.% NaCl solution. In the present study, a high-performance PU/Gr composite coating is developed and characterized to obtain coatings with multifunctional properties, such as combined high corrosion resistance and antifriction properties, for extending the coating lifetime in outdoor and marine environments. We prepare PU composite coatings with higher concentrations (2, 4 and 8 wt.%) of Gr sheets and systematically study their corrosion resistance and antifriction properties. Moreover, we focus on the analysis of the anticorrosion behaviors of PU/Gr composite coatings by using EIS and SST techniques. The antifriction properties of the coatings are discussed based on their COF values and the mechanical properties.

2. Experimental

2.1. Materials

The steel substrates purchased from Q-Lab Co. were R-46-I type (R-46-I, Q-Lab Co., Westlake, OH, USA) with dimensions 4 in × 6 in × 0.032 in. Commercial PU resin (type: UT-UR-176N, OH Number: 46–50) and hardener (Desmodur N3390) were obtained from Yuta Resin Chemical Co. Ltd (Tainan, Taiwan) and Bayer Co. (Leverkusen, Germany), respectively. The solid content of PU resin was 60%. Also, the viscosity of the PU resin was 350 cps. The weight ratio of the PU resin to the hardener was 3:1. The Gr sheet (type: P-ML20; specific surface area: 25 m²·g⁻¹; average thickness: 5 nm) were purchased from Enerage, Inc. (Yilan, Taiwan). PU/Gr composites coatings were fabricated by Lingo Industrial Co. Ltd (Taoyuan, Taiwan) through mechanical mixing by using a multipurpose mixer with a defoaming function. The best dispersion of Gr powder in PU resins was achieved with a Gr content of 8 wt.%, as suggested by Lingo Industrial Co. Ltd. Therefore, three PU/Gr composite coatings with different Gr contents of 0, 2, 4 and 8 wt.% were prepared and the dispersion was milled to obtain 10 μm fineness. The viscosity of PU coatings containing 2, 4 and 8 wt.% Gr powders was 2000 ± 1000, 9000 ± 1000 and 20,000 ± 2000 cps, respectively.

2.2. Sample Preparation

Prior to the application of the coating, substrates were cleaned in an ultrasonic bath with acetone for 10 min and then air dried. PU coatings containing 0, 2, 4 and 8 wt.% Gr powders, which were designated as PU, PU2, PU4 and PU8, respectively, were applied on the substrate by using a wire-wound lab rod. The prepared coating samples were cured at room temperature overnight and then postcured at 80 °C for 1 h in an oven (Deng YNG, New Taipei City, Taiwan) to ensure they were completely dry before measurements. The dry film thickness of all coatings was controlled to be within the range of 30 to 35 μm, as measured using an Elcometer 456 dry film thickness gauge (Manchester, UK).

2.3. Characterization

The surface morphology of the coating samples was observed using a scanning electron microscope (SEM) (JEOL JSM-6510, Tokyo, Japan) at a facility in National Taiwan University. EIS was performed to assess the corrosion resistance of the prepared coating samples. The impedance spectra of the samples were measured in a standard three-electrode system three-electrode cell. The counter electrode was a graphite rod and the reference electrode was a saturated calomel electrode. All EIS measurements were conducted in 3.5 wt.% of NaCl solution by using a Gamry Reference 600 potentiostat (Warminster, PA, USA). EIS measurements were recorded at an open-circuit potential in the frequency range of 10⁵ to 10⁻² Hz by using an alternating current amplitude of 10 mV. The tested area of the coating samples in all electrochemical tests was 7.8 cm². To confirm the reproducibility of EIS results, three pieces of each coated sample were measured. In addition, SST was conducted to further validate the corrosion protection performance of the coating samples. The coating samples were placed at a tilted angle of 30° in a chamber containing 5 wt.% of NaCl fog according to the ASTM B117 standard [45]. The antifriction properties of the coatings were determined using a ball-on-disc tribometer (CSM, Needham, MA, USA) under the following conditions: load of 2 N, sliding velocity of 2 cm·s⁻¹, friction duration of 50 min and wear track length of 60 m. GCr 15 steel balls with a diameter of 6 mm were used as the counterpart. All experiments were performed under dry conditions. Dynamic mechanical analysis (DMA) was performed using DMA Q800 (TA Instruments Co., New Castle, DE, USA) at a frequency of 10 Hz, a heating rate of 10 °C·min⁻¹ and a scanning temperature range of -20 to 30 °C in the tensile mode. For this measurement, PU and PU/Gr composite coatings were cut into samples of the following dimensions: 15 mm in length, 5 mm in width and 1 mm in thickness. The thermal conductivity measurements were performed using a thermal constants analyzer (Hot Disk TPS 2500S, Gothenburg, Sweden).

3. Results and Discussion

3.1. Morphologies of PU/Gr Composite Coatings

The typical top-view SEM images of the PU and PU/Gr composite coatings with different Gr ratios are shown in Figure 1a–d. The PU sample had a relatively smooth and homogeneous surface morphology (Figure 1a). Little changes were observed in the surface morphology of the coating when it was modified with 2 wt.% of Gr. The PU2 sample appeared slightly rugged (Figure 1b). In the cases of the PU 4 and PU8 samples, the surface morphology became rougher as the Gr content in the PU coating was increased to 8 wt.% (Figure 1d). On the basis of the top-view SEM images of the coatings, no crack or obvious defect was observed on the top surface of each coating sample.

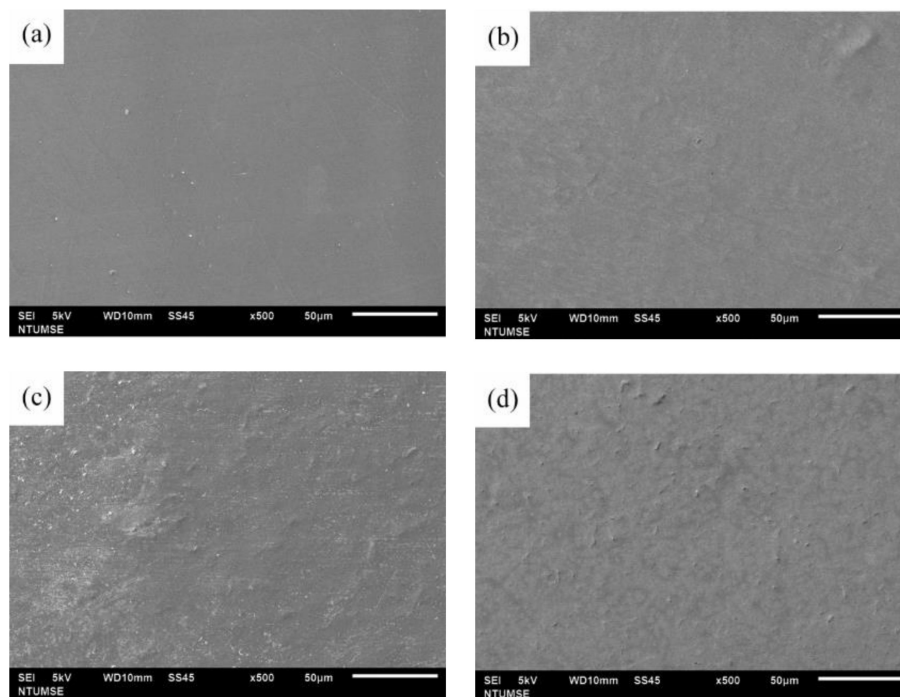


Figure 1. Scanning electron microscopy (SEM) images of coating samples: (a) Polyurethane (PU), (b) PU2, (c) PU4 and (d) PU8.

3.2. Corrosion Resistance of PU/Gr Composite Coatings

The corrosion performance of the PU coating and several PU/Gr composite coatings on the steel substrate was evaluated through EIS. EIS is a nondestructive measurement technique used for assessing the durability of organic coatings in aqueous environments [46]. EIS can provide information regarding the barrier properties and water uptake of organic coatings, as well as can be used to characterize the degradation process before visual damage to the coating. Figure 2 shows the Bode magnitude and phase plots obtained for different durations of immersion in 3.5 wt.% of NaCl solution. Initially, the Bode plots of all the PU/Gr composite coating samples were close to a straight line with a negative slope over the entire test frequency range. This implied that the PU2, PU4 and PU8 coatings behaved as favorable barriers early into the measurement. By contrast, the PU sample showed a resistive plateau corresponding to the charge transfer associated with corrosion at low frequencies in Bode plots on the first day of the experiment (Figure 2a). This resistive plateau was also found in the Bode plot of the PU2 sample on the 7th day of immersion. According to its Bode plots, the PU4 and PU8 samples retained their capacitive behavior and no clear plateau was observed even after 28 days of immersion.

The impedance value in a low-frequency range ($|Z|_{0.01\text{Hz}}$) in Bode plots may be an appropriate indicator for characterizing the corrosion protection performance of organic coatings [47]. A large and stable $|Z|_{0.01\text{Hz}}$ value usually indicates satisfactory corrosion protection performance. As shown in Figure 2, the $|Z|_{0.01\text{Hz}}$ values of all the samples were higher than $10^8 \Omega \cdot \text{cm}^2$ on the first day of immersion. However, the $|Z|_{0.01\text{Hz}}$ values of the PU and PU2 samples decreased significantly by at least two orders of magnitude after 7 days of immersion. The decrease in the $|Z|_{0.01\text{Hz}}$ values of the PU and PU2 samples indicated an increase in the delaminated area, possibly due to the establishment of water and electrolyte pathways through the coatings. Once water reaches the coating–substrate interface, the corrosion of the metal may start. By contrast, the $|Z|_{0.01\text{Hz}}$ value of PU4 and PU8 samples decreased only slightly (Figure 2c–d). This stable evolution of the $|Z|_{0.01\text{Hz}}$ value suggested that the PU coating containing higher amounts of Gr of up to 8 wt.% can act as a barrier against water and electrolytes.

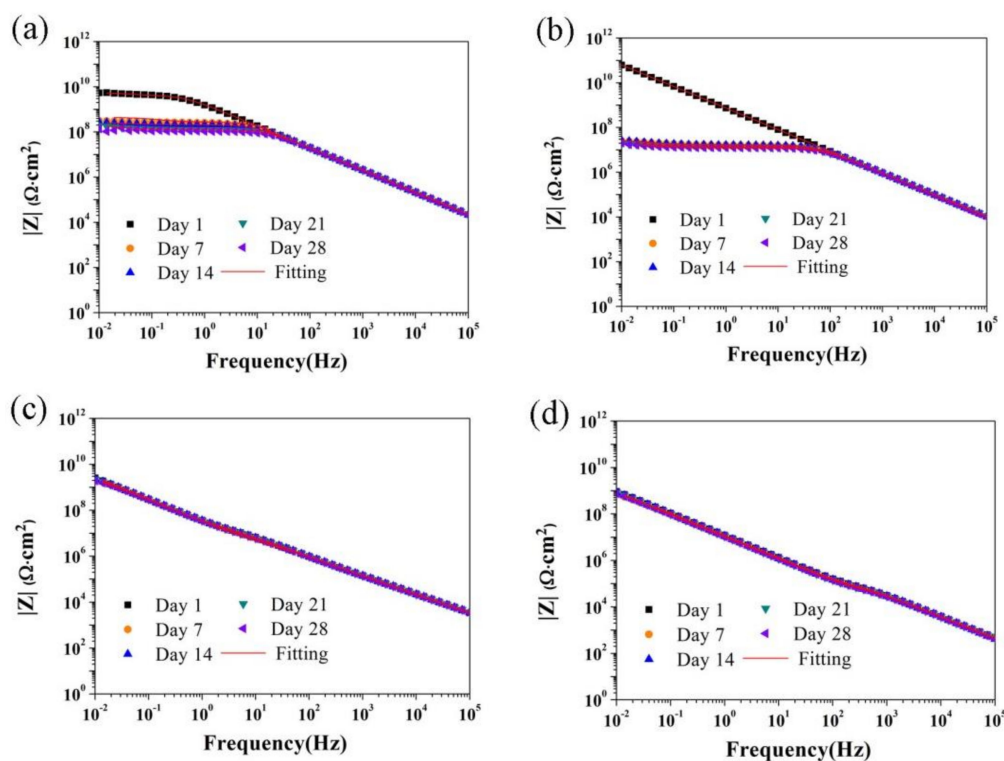


Figure 2. Bode plots of (a) PU, (b) PU2, (c) PU4 and (d) PU8 immersed in 3.5 wt.% NaCl solution for different durations.

To study the effect of Gr addition on the corrosion resistance of PU coatings, equivalent electric circuits were used to interpret the measured impedance data. In this study, equivalent electric circuits (Figure 3) were employed to fit the measured Bode plots by using the ZSimpWin software [38,39,48]. R_s denotes the solution resistance. R_{pore} and CPE_c are the pore resistance and constant phase element of the coating, respectively. R_{ct} and CPE_{dl} represent the charge transfer resistance of the corroded area at the coating–substrate interface and the double layer capacitance, respectively. Figure 4 shows variations in R_{pore} with immersion time in NaCl solution. The R_{pore} value, which reflects the ability to resist electrolyte penetration, is a valuable parameter used to evaluate the protective performance of coatings. As shown in Figure 3a, the R_{pore} value of the PU sample decreased gradually by one order of magnitude (from 7.72×10^8 to $3.83 \times 10^7 \Omega \cdot \text{cm}^2$) after 28 days of immersion. A sharp drop of five orders of magnitude in the value of R_{pore} (from 1.30×10^{12} to $4.93 \times 10^7 \Omega \cdot \text{cm}^2$) after 7 days of immersion was observed in the case of the PU2 sample. This decrease in the R_{pore} value can be explained by the ingress of water and the development of ionic conducting pathways (pores

or microcracks) in the coating [49,50]. The phenomenon of water uptake was confirmed based on variations in the coating capacitance value. A small variation in the R_{pore} value was observed in the cases of the PU4 and the PU8 samples and their value remained at $10^9 \Omega \cdot \text{cm}^2$ over the entire immersion period. Consequently, the decrease in the R_{pore} values of the PU and PU2 samples indicated their limited anticorrosion performance. By contrast, the PU4 and PU8 samples retained their R_{pore} value over 28 days of immersion. The stable R_{pore} value of the PU4 and PU8 samples can be attributed to the fact that a sufficient amount of Gr can act as a physical barrier and complicate the diffusion pathways of corrosive species (Figure 5).

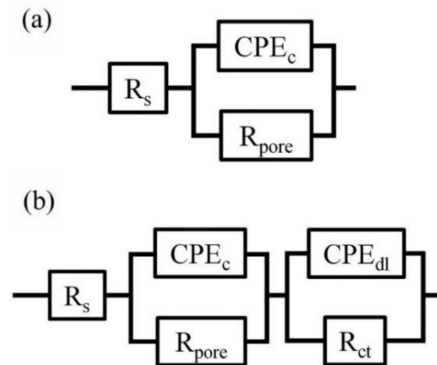


Figure 3. Equivalent circuits with (a) one time constant and (b) use of two time constants for fitting electrochemical impedance spectroscopy (EIS) data of coating samples.

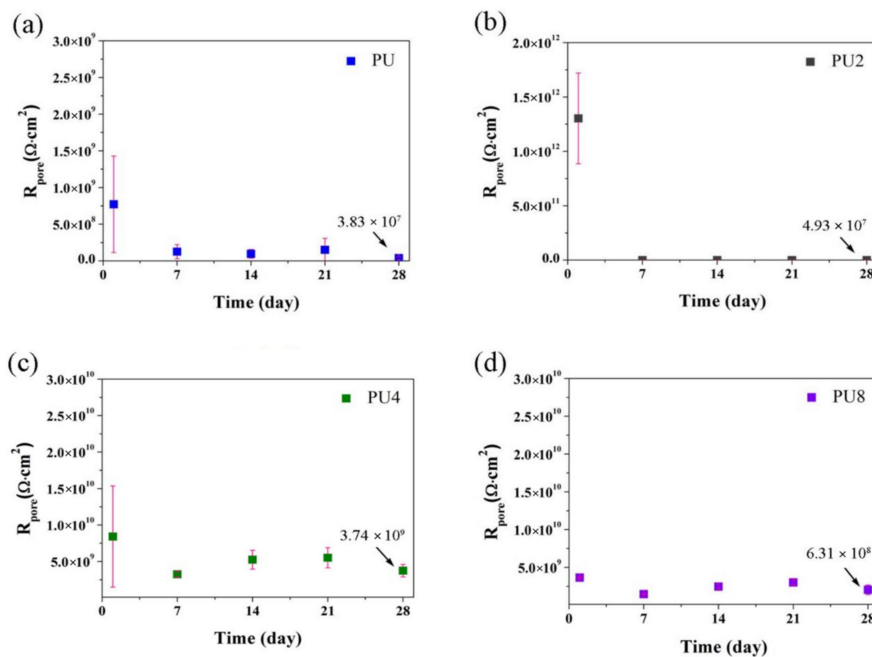


Figure 4. Evolution of R_{pore} of various coating samples during 28 days of immersion in 3.5 wt.% NaCl solution: (a) PU, (b) PU2, (c) PU4 and (d) PU8.

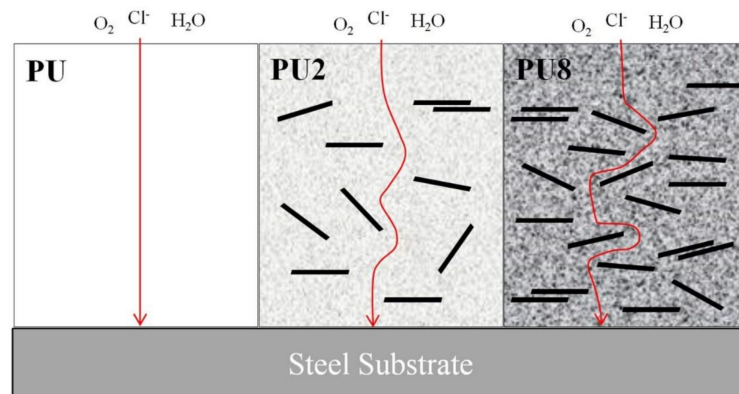


Figure 5. Schematic diagram of effect of Gr addition on barrier and corrosion protection performance of PU coating.

The coating capacitance extracted from EIS data by using equivalent electric circuit fitting is used to determine the lifetime of organic coatings in aqueous media. By studying the variation of coating capacitance, it is possible to evaluate the water uptake phenomenon because the presence of even a very small amount of water can modify the dielectric constant of the polymer [51,52]. The presence of water in the coating can activate the corrosion process or lead to loss of adhesion and blistering [52]. Therefore, the evolution of coating capacitance is among the important parameters for characterizing the protective properties of organic coatings. Usually, the lower the coating capacitance, the better is the barrier performance and the higher is the corrosion resistance. The true value of coating capacitance is extracted from CPE by using the following equation [53–55]:

$$C = Q^{\frac{1}{n}} \times R^{\frac{(1-n)}{n}}$$

where Q represents the magnitude of CPE and n is the exponent of CPE. R is the resistance in parallel with CPE. Figure 6 shows that the initial coating capacitance of the PU2 sample is lower than that of the PU, PU4 and PU8 samples. However, the coating capacitance of the PU2 sample increased rapidly and reached a high value after 7 days of immersion. This huge increase is probably because of the defect capacitance and the increasing water content in the coating because of its high dielectric constant (80.4) [46,53,56]. The trend of increasing coating capacitance with increasing immersion time was also observed in case of the PU coating. The change in coating capacitance was negligible and the value remained at $10^{-9} \text{ F cm}^{-2}$ in cases of the PU4 and PU8 samples throughout the immersion period, indicating that only a small amount of water was absorbed by the coating. Overall, high pore resistance is associated with low coating capacitance and the steady evolution of these two parameters revealed that the PU4 and PU8 coatings can act as a more effective barrier against attacks by aggressive media.

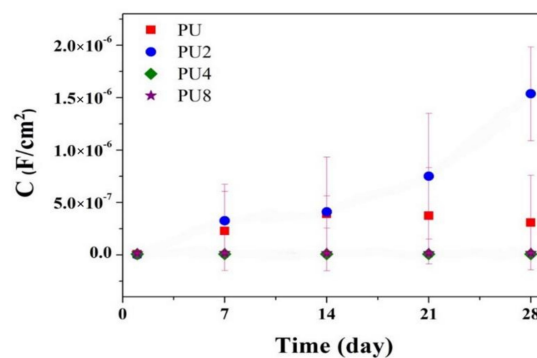


Figure 6. Evolution of coating capacitance of various coating samples during 28 days of immersion in 3.5 wt.% NaCl solution.

3.3. SST

In addition to electrochemical tests, the SST was conducted to evaluate the corrosion performance of the coatings. SST is a standard and useful test for assessing the corrosion resistance of coating samples. After the test, the appearance of coated samples was evaluated. The photographs of the coating samples after exposure in the salt spray chamber for up to 28 days are shown in Figure 7. After 5 days of exposure, a few black corrosion spots could be seen clearly on the PU sample, as indicated by red arrows in Figure 7a. As the exposure time increased to 21 days, a few blisters (indicated by yellow arrows in Figure 7b) appeared on the PU2 sample due to solvent retention. A higher density of blisters was found on the PU2 sample when exposure time was increased to 28 days, suggesting the enrichment of water, oxygen and corrosion ions at the coating–substrate interface, leading to the initiation of severe delamination of the coating. By contrast, in cases of the PU4 and PU8 samples (Figure 7c–d), no apparent corrosion spots and blisters were observed even after 28 days of exposure. The SST findings are consistent with previous EIS results, indicating that the composite coatings containing 4 and 8 wt.% of Gr have better barrier properties. These results can be attributed to the fact that the addition of a sufficient amount of Gr to PU coating can block the paths of water and oxygen to the extent that they barely penetrate through to the base metal.

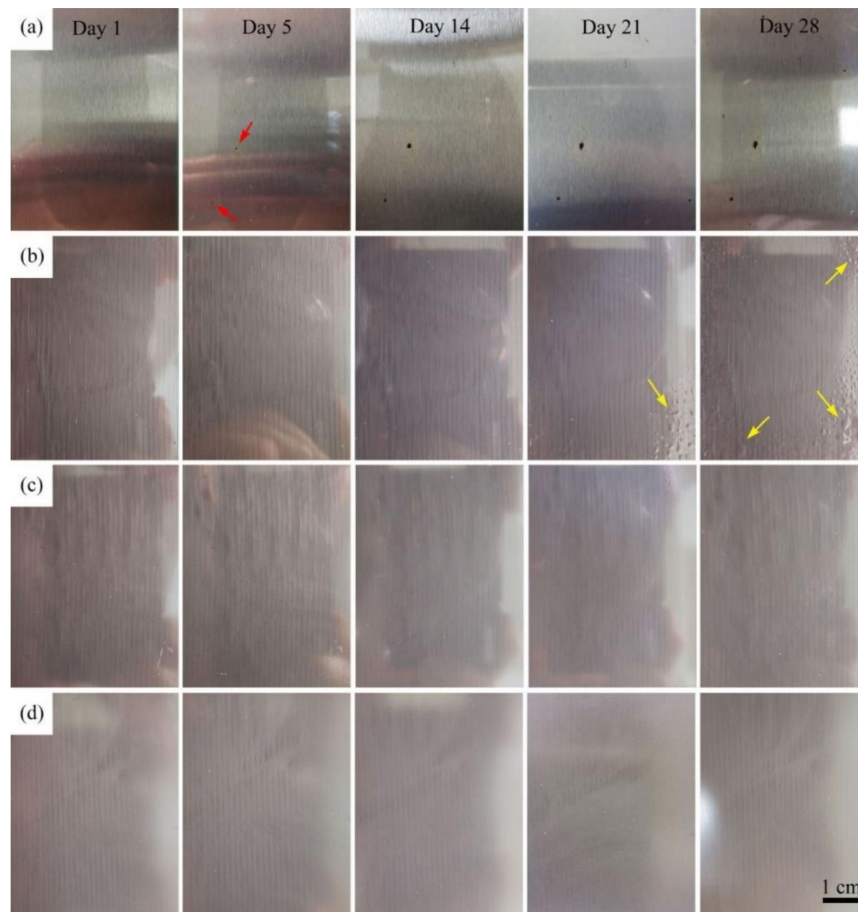


Figure 7. Visual appearance of coating samples after different exposure times in salt spray chamber: (a) PU, (b) PU2, (c) PU4 and (d) PU8.

3.4. Adhesion of Composite Coatings by the Cross-Cut Tape Test

Adhesion performance is one of the most important properties of protective coatings [57–60]. Therefore, in this study, the ASTM cross-cut tape test was performed to evaluate the effect of Gr addition on the adhesion of the composite coating to steel panels. The grade of adhesion quality in

the test was rated from 0B to 5B, and 5B and 0B represent the best and poorest adhesion performance, respectively. Figure 8 shows the photographs of the PU coating and composite coatings containing different Gr ratios after the cross-cut tape test. As shown in Figure 8a, some peeling of the coating from the grid area and chipping around the cut lines were observed. This coating was rated as 3B by referring to the ASTM D 3359 standard [61]. By contrast, as shown in Figure 8b–d, the edges of the cut lines were smooth and very little to no removal of the coating was observed, indicating strong coating adhesion. These results indicate that the coatings containing Gr can bind strongly to the surface of steel. The strong adhesion of Gr-containing coatings to the substrate in the present case might be attributed to the fact that the addition of Gr modifies the physical properties of PU/Gr composite coatings such that the internal stress induced at the coating–substrate interface because of variations in temperature during the curing process is relaxed and reduced [37]. Therefore, the addition of Gr can improve the interfacial bond established between the composite coating and the substrate, leading to enhanced corrosion resistance.

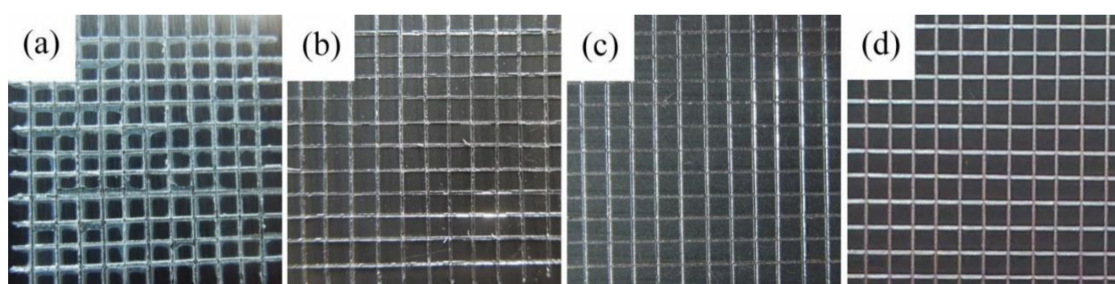


Figure 8. Appearance of cross-cut surface before application of tape: (a) PU, (b) PU2, (c) PU4 and (d) PU8.

3.5. Antifriction Properties and COF Analysis

Figure 9 shows the COF evolution of the PU coatings containing different concentrations of Gr under the dry sliding condition. There are two antifriction behaviors related to sliding performance. The COF of the PU sample first increased rapidly and reached 0.5 after a sliding distance of less than 0.2 m and then it increased steadily with increasing sliding distance until it reached 0.64 at the end of the test. The increase of COF may be associated with ploughing process because of roughening and/or trapped wear particles which will change the real area of contact and hence the friction [62]. The COF curves of the PU2 and PU samples had similar shapes but the COF of the PU2 sample was slightly lower than that of the PU sample. This suggested that the addition of 2 wt.% of Gr to the PU coating had a minor effect on the antifriction behavior of the coating. However, the COF of the PU4 and PU8 samples showed a sharp increase followed by a sharp decrease, stabilizing subsequently with the passage of measurement time. Moreover, the COF of the PU4 and PU8 samples decreased significantly compared with that of the PU coating after sliding for 60 m. The presence of COF fluctuation observed on the PU4 and PU8 samples was possibly due to the generation of Gr-containing hard wear debris within the sliding contact interface. Based on the average COF in the steady stage, a maximum friction reduction of 61% was achieved from 0.58 of the neat PU sample to 0.23 of the PU8 sample. This decrement in the COF of the composite coating can be attributed to the lubricating effect of the presence of sufficient amount of Gr in the sliding surface.

It is well known that friction is a typical dissipative process in which mechanical energy is converted into heat [62]. For composite materials, this energy dissipation can occur by the microstructural slippage at the interface between the filler surface and the polymer matrix, resulting in transformation of mechanical energy into heat through an internal friction process. The addition of Gr into PU coatings strongly influences the dynamics of polymer chains and their thermal properties, including the loss modulus (E''). E'' is a measure of the energy dissipated between polymer chains and a filler and it is closely related to acoustic absorption behavior [63–65]. Consequently, DMA

was performed in the present study to evaluate E'' of the PU coating and the PU/Gr composite coatings as a function of temperature. Figure 10 shows the loss modulus (E'') of the PU coating and the PU/Gr composite coatings. The incorporation of Gr enhanced the E'' value. Moreover, as the Gr content increased, the E'' value of the composite coatings increased over the entire temperature range. Compared with the PU coating (123.5 MPa), the E'' values of PU2, PU4 and PU8 at the ambient temperature (25 °C) were 283.2, 381.1 and 439.2 MPa, respectively, which indicated substantial increases of approximately 129%, 208% and 255%, respectively. The E'' values represent the ability of a material to dissipate mechanical energy through molecular motion [57,65]. Thus, the marked increase in the E'' value was attributed to large frictional energy dissipation caused by the high specific surface ratio of Gr. Furthermore, the thermal conductivity of the coatings is another significant evidence for explaining differences in their antifriction behaviors. The thermal conductivities of the PU and PU/Gr composite coatings measured using a thermal constants analyzer are listed in Table 1. As mentioned above, the friction mechanisms depend strongly on the thermal effects between materials at actual contact spots. A large amount of frictional heat was produced and the interface temperature increased greatly when a polymer coating was subjected to sliding for a certain period. An increase in the interface temperature causes thermal softening, leading to severe plastic deformation of the polymer coating [66]. As shown in Table 1, the thermal conductivity of the coatings increased with increasing Gr content owing to their superior thermal conductivity ($5000 \text{ W}\cdot\text{mK}^{-1}$) [67]. Thus, the enhancement of this property is beneficial for increasing the conduction and dissipation of frictional heat. As a result, thermal softening would not occur in the worn area, which increases resistance to wear. These findings can be used to demonstrate the effects of Gr addition on the antifriction properties of PU coatings and support the COF results that the PU 8 sample had the best antifriction properties in this study.

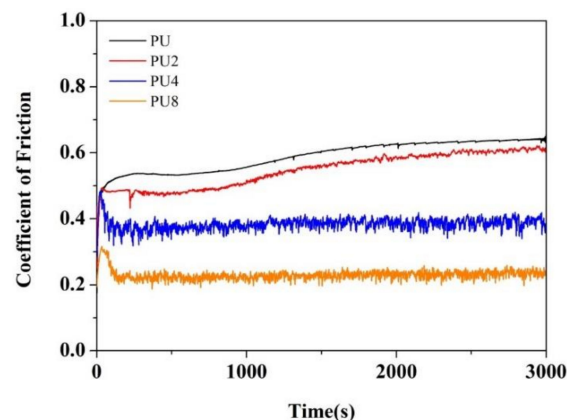


Figure 9. Coefficient of friction versus sliding time for PU coating and PU/Gr composite coatings.

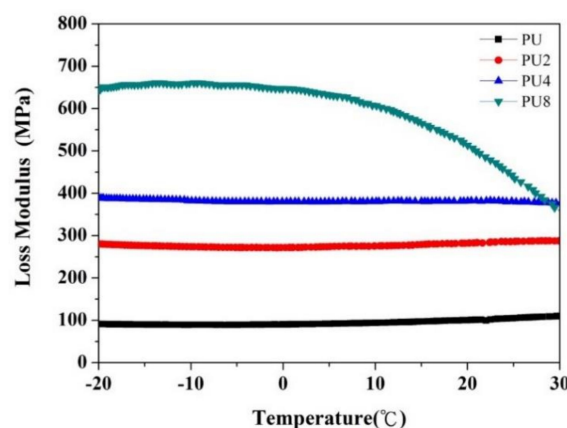


Figure 10. Loss moduli of PU coating and PU/Gr composite coatings.

Table 1. Thermal conductivity of PU coating and PU/Gr composite coatings.

Coatings	Thermal Conductivity ($W \cdot mK^{-1}$)
PU	0.226
PU2	0.356
PU4	0.573
PU8	1.151

4. Conclusions

In the present study, high-performance PU/Gr composite coatings with excellent corrosion and antifriction properties were developed. The effects of adding Gr into a PU coating on the corrosion resistance and antifriction properties of the coating were investigated systematically. We found that determining a sufficient Gr content is crucial for enhancing not only the corrosion resistance but also the antifriction properties of PU/Gr composite coatings. The main conclusions can be summarized as follows:

- Corrosion results obtained using EIS indicated that the $|Z|_{0.01Hz}$ value, pore resistance and coating capacitance of the PU coatings containing 4 and 8 wt.% of Gr exhibited stable evolution during 28-day immersion in 3.5 wt.% of NaCl solution.
- SST results revealed that the PU4 and PU8 coatings decelerated the corrosion rate and enhanced long-term corrosion protection.
- The loss modulus and thermal conductivity of the PU coating increased with the Gr content owing to the strong frictional energy dissipation effect and the superior thermal conductivity of Gr.
- The addition of Gr to neat PU coating reduced the COF of the PU/Gr composite coatings. Our results indicated that the PU 8 sample had excellent antifriction properties. The COF value of the PU8 coating was 61% lower than that of the neat PU coating.
- Incorporating 8 wt.% Gr into the PU coating led to enhanced anticorrosion properties and this coating exhibited the best antifriction behaviors.

Author Contributions: Conceptualization, Y.-L.L.; Methodology, P.-Y.T. and Y.-L.L.; Validation, P.-Y.T. and T.-E.C.; Formal Analysis, P.-Y.T. and Y.-L.L.; Investigation, P.-Y.T. and T.-E.C.; Writing-Original Draft Preparation, P.-Y.T.; Writing-Review & Editing, Y.-L.L.; Supervision, Y.-L.L.

Funding: This research was funded by the Ministry of Science and Technology, Taiwan, under Grant No. MOST 105-2221-E-002-115.

Acknowledgments: We acknowledge Yu-Jie Jhou and Chih-Chien Hung for providing technical assistance and valuable contributions.

Conflicts of Interest: The authors declare no conflict of interest.

References

1. Dhoke, S.K.; Khanna, A.S.; Sinha, T.J.M. Effect of nano-ZnO particles on the corrosion behavior of alkyd-based waterborne coatings. *Prog. Org. Coat.* **2009**, *64*, 371–382. [[CrossRef](#)]
2. Shi, X.; Nguyen, T.A.; Suo, Z.; Liu, Y.; Avci, R. Effect of nanoparticles on the anticorrosion and mechanical properties of epoxy coating. *Surf. Coat. Technol.* **2009**, *204*, 237–245. [[CrossRef](#)]
3. Zhang, X.; Wang, F.; Du, Y. Effect of nano-sized titanium powder addition on corrosion performance of epoxy coatings. *Surf. Coat. Technol.* **2007**, *201*, 7241–7245. [[CrossRef](#)]
4. Shao, Y.; Jia, C.; Meng, G. The role of a zinc phosphate pigment in the corrosion of scratched epoxy-coated steel. *Corros. Sci.* **2009**, *51*, 371–379. [[CrossRef](#)]
5. Sababi, M.; Pan, J.; Augustsson, P.-E.; Sundell, P.-E.; Claesson, P.M. Influence of polyaniline and ceria nanoparticle additives on corrosion protection of a UV-cure coating on carbon steel. *Corros. Sci.* **2014**, *84*, 189–197. [[CrossRef](#)]

6. Chen, Y.; Zhao, S.; Chen, M.; Zhang, W.; Mao, J.; Zhao, Y.; Maitz, M.F.; Huang, N.; Wan, G. Sandwiched polydopamine (PDA) layer for titanium dioxide (TiO₂) coating on magnesium to enhance corrosion protection. *Corros. Sci.* **2015**, *96*, 67–73. [[CrossRef](#)]
7. Ramezanzadeh, B.; Niroumandrad, S.; Ahmadi, A.; Mahdavian, M.; Moghadam, M.M. Enhancement of barrier and corrosion protection performance of an epoxy coating through wet transfer of amino functionalized graphene oxide. *Corros. Sci.* **2016**, *103*, 283–304. [[CrossRef](#)]
8. Sun, W.; Wang, L.; Wu, T.; Pan, Y.; Liu, G. Communication—Multi-Layer Boron Nitride Nanosheets as Corrosion-Protective Coating Fillers. *J. Electrochem. Soc.* **2016**, *163*, C16–C18. [[CrossRef](#)]
9. Niroumandrada, S.; Rostamib, M.; Ramezanzadeh, B. Effects of combined surface treatments of aluminium nanoparticle on its corrosion resistance before and after inclusion into an epoxy coating. *Prog. Org. Coat.* **2016**, *101*, 486–501. [[CrossRef](#)]
10. Yeh, J.M.; Yao, C.T.; Hsieh, C.F.; Lin, L.H.; Chen, P.L.; Wu, J.C.; Yang, H.C.; Wu, C.P. Preparation, characterization and electrochemical corrosion studies on environmentally friendly waterborne polyurethane/Na⁺-MMT clay nanocomposite coatings. *Eur. Polym. J.* **2008**, *44*, 3046–3056. [[CrossRef](#)]
11. Deyaba, M.A.; Ouarsalb, R.; Al-Sabagha, A.M.; Lachkarb, M.; el Balib, B. Enhancement of corrosion protection performance of epoxy coating by introducing new hydrogenphosphate compound. *Prog. Org. Coat.* **2017**, *107*, 37–42. [[CrossRef](#)]
12. Cui, M.; Ren, S.; Chen, J.; Liu, S.; Zhang, G.; Zhao, H.; Wang, L.; Xuea, Q. Anticorrosive performance of waterborne epoxy coatings containing water-dispersible hexagonal boron nitride (h-BN) nanosheets. *Appl. Surf. Sci.* **2017**, *397*, 77–86. [[CrossRef](#)]
13. Caldona, E.B.; de Leon, A.C.C.; Pajarito, B.B.; Advincula, R.C. Novel anti-corrosion coatings from rubber-modified polybenzoxazine-based polyaniline composites. *Appl. Surf. Sci.* **2017**, *422*, 162–171. [[CrossRef](#)]
14. Gharagozloua, M.; Ramezanzadehb, B.; Baradarana, Z. Synthesize and characterization of a novel anticorrosive cobalt ferrite nanoparticles dispersed in silica matrix (CoFe₂O₄-SiO₂) to improve the corrosion protection performance of epoxy coating. *Appl. Surf. Sci.* **2016**, *377*, 86–98. [[CrossRef](#)]
15. Palimi, M.J.; Alibakhshi, E.; Bahlakeh, G.; Ramezanzadeh, B.; Mahdavian, M. Electrochemical Investigations of the Corrosion Protection Properties of an Epoxy-Ester Coating Filled with Cerium Acetyl Acetate Anticorrosive Pigment. *J. Electrochem. Soc.* **2017**, *164*, C709–C716. [[CrossRef](#)]
16. Song, D.; Yin, Z.; Liu, F.; Wan, H.; Gao, J.; Zhang, D.; Li, X. Effect of carbon nanotubes on the corrosion resistance of water-borne acrylic coatings. *Prog. Org. Coat.* **2017**, *110*, 182–186. [[CrossRef](#)]
17. Shen, W.; Feng, L.; Liu, X.; Luo, H.; Liu, Z.; Tong, P.; Zhang, W. Multiwall carbon nanotubes-reinforced epoxy hybrid coatings with high electrical conductivity and corrosion resistance prepared via electrostatic spraying. *Prog. Org. Coat.* **2016**, *90*, 139–146. [[CrossRef](#)]
18. Deyab, M.A. Effect of carbon nano-tubes on the corrosion resistance of alkyd coating immersed in sodium chloride solution. *Prog. Org. Coat.* **2015**, *85*, 146–150. [[CrossRef](#)]
19. Yu, Y.H.; Lin, Y.Y.; Lin, C.H.; Chana, C.C.; Huang, Y.C. High-performance polystyrene/graphene-based nanocomposites with excellent anti-corrosion properties. *Polym. Chem.* **2014**, *5*, 535–550. [[CrossRef](#)]
20. Chang, C.H.; Huang, T.C.; Peng, C.W.; Yeh, T.C.; Lu, H.I.; Hung, W.I.; Weng, C.J.; Yang, T.I.; Yeh, J.M. Novel anticorrosion coatings prepared from polyaniline/graphene composites. *Carbon* **2012**, *50*, 5044–5051. [[CrossRef](#)]
21. Chang, K.C.; Ji, W.F.; Lai, M.C.; Hsiao, Y.R.; Hsu, C.H.; Chuang, T.L.; Wei, H.; Yeh, J.M.; Liu, W.R. Synergistic effects of hydrophobicity and gas barrier properties on the anticorrosion property of PMMA nanocomposite coatings embedded with graphene nanosheets. *Polym. Chem.* **2014**, *5*, 1049–1056. [[CrossRef](#)]
22. Li, Y.; Yang, Z.; Qiu, H.; Dai, Y.; Zheng, Q.; Li, J.; Yang, J. Self-aligned graphene as anticorrosive barrier in waterborne polyurethane composite coatings. *J. Mater. Chem. A* **2014**, *2*, 14139–14145. [[CrossRef](#)]
23. Hayatgheib, Y.; Ramezanzadeh, B.; Kardar, P.; Mahdavian, M. A comparative study on fabrication of a highly effective corrosion protective system based on graphene oxide-polyaniline nanofibers/epoxy composite. *Corros. Sci.* **2018**, *133*, 358–373. [[CrossRef](#)]
24. Liu, S.; Gu, L.; Zhao, H.; Chen, J.; Yu, H. Corrosion Resistance of Graphene-Reinforced Waterborne Epoxy Coatings. *J. Mater. Sci. Technol.* **2016**, *32*, 425–431. [[CrossRef](#)]
25. Li, J.; Cui, J.; Yang, J.; Li, Y.; Qiu, H.; Yang, J. Reinforcement of graphene and its derivatives on the anticorrosive properties of waterborne polyurethane coatings. *Compos. Sci. Technol.* **2016**, *129*, 30–37. [[CrossRef](#)]

26. Li, J.; Cui, J.; Yang, J.; Ma, Y.; Qiu, H.; Yang, J. Silanized graphene oxide reinforced organofunctional silane composite coatings for corrosion protection. *Prog. Org. Coat.* **2016**, *99*, 443–451. [[CrossRef](#)]
27. Yu, Z.; Di, H.; Ma, Y.; Pan, L.L.Y.; Zhang, C.; He, Y. Fabrication of graphene oxide–alumina hybrids to reinforce the anti-corrosion performance of composite epoxy coatings. *Appl. Surf. Sci.* **2015**, *351*, 986–996. [[CrossRef](#)]
28. Pourhashem, S.; Vaezi, M.R.; Rashidi, A.; Bagherzadeh, M.R. Distinctive roles of silane coupling agents on the corrosion inhibition performance of graphene oxide in epoxy coatings. *Prog. Org. Coat.* **2017**, *111*, 47–56. [[CrossRef](#)]
29. Pourhashem, S.; Rashidi, A.; Vaezi, M.R.; Bagherzadeh, M.R. Excellent corrosion protection performance of epoxy composite coatings filled with amino-silane functionalized graphene oxide. *Surf. Coat. Technol.* **2017**, *317*, 1–9. [[CrossRef](#)]
30. Pourhashem, S.; Vaezi, M.R.; Rashidi, A. Investigating the effect of SiO₂-graphene oxide hybrid as inorganic nanofiller on corrosion protection properties of epoxy coatings. *Surf. Coat. Technol.* **2017**, *311*, 282–294. [[CrossRef](#)]
31. Xue, B.; Yu, M.; Liu, J.; Li, S.; Xiong, L.; Kong, X. Corrosion Protective Properties of Silane Functionalized Graphene Oxide Film on AA2024-T3 Aluminum Alloy. *J. Electrochem. Soc.* **2016**, *163*, C798–C806. [[CrossRef](#)]
32. Zhou, P.; Li, W.; Zhu, X.; Li, Y.; Jin, X.; Chen, J. Graphene Containing Composite Coatings as a Protective Coatings against Hydrogen Embrittlement in Quenching & Partitioning High Strength Steel. *J. Electrochem. Soc.* **2016**, *163*, D160–D166. [[CrossRef](#)]
33. Dong, Y.; Liu, Q.; Zhou, Q. Corrosion behavior of Cu during graphene growth by CVD. *Corros. Sci.* **2014**, *89*, 214–219. [[CrossRef](#)]
34. Yoo, B.M.; Shin, H.J.; Yoon, H.W.; Park, H.B. Graphene and graphene oxide and their uses in barrier polymers. *J. Appl. Polym. Sci.* **2014**, *131*, 39628. [[CrossRef](#)]
35. Xiong, J.; Zheng, Z.; Qin, X.; Li, M.; Li, H.; Wang, X. The thermal and mechanical properties of a polyurethane/multi-walled carbon nanotube composite. *Carbon* **2006**, *44*, 2701–2707. [[CrossRef](#)]
36. Thostenson, E.T.; Ren, Z.; Chou, T.-W. Advances in the science and technology of carbon nanotubes and their composites: A review. *Compos. Sci. Technol.* **2001**, *61*, 1899–1912. [[CrossRef](#)]
37. Khun, N.W.; Frankel, G.S. Cathodic delamination of polyurethane/multiwalled carbon nanotube composite coatings from steel substrates. *Prog. Org. Coat.* **2016**, *99*, 55–60. [[CrossRef](#)]
38. Mo, M.; Zhao, W.; Chen, Z.; Yu, Q.; Zeng, Z.; Wu, X.; Xue, Q. Excellent tribological and anti-corrosion performance of polyurethane composite coatings reinforced with functionalized graphene and graphene oxide nanosheets. *RSC Adv.* **2015**, *5*, 56486–56497. [[CrossRef](#)]
39. Liu, D.; Zhao, W.; Liu, S.; Cen, Q.; Xue, Q. Comparative tribological and corrosion resistance properties of epoxy composite coatings reinforced with functionalized fullerene C60 and grapheme. *Surf. Coat. Technol.* **2016**, *286*, 354–364. [[CrossRef](#)]
40. Chen, C.; Qiu, S.; Cui, M.; Qin, S.; Yan, G.; Zhao, H.; Wang, L.; Xue, Q. Achieving high performance corrosion and wear resistant epoxy coatings via incorporation of noncovalent functionalized grapheme. *Carbon* **2017**, *114*, 356–366. [[CrossRef](#)]
41. Bandeira, P.; Monteiro, J.; Baptista, A.M.; Magalhaes, F.D. Influence of oxidized graphene nanoplatelets and [DMIM][NTf₂] ionic liquid on the tribological performance of an epoxy-PTFE coating. *Tribol. Int.* **2016**, *97*, 478–489. [[CrossRef](#)]
42. Xia, S.; Liu, Y.; Pei, F.; Zhang, L.; Gao, Q.; Zou, W.; Peng, J.; Cao, S. Identical steady tribological performance of graphene-oxide-strengthened polyurethane/epoxy interpenetrating polymer networks derived from graphene nanosheet. *Polymer* **2015**, *64*, 62–68. [[CrossRef](#)]
43. Li, G.; Feng, L.; Tong, P.; Zhai, Z. The properties of MWCNT/polyurethane conductive composite coating prepared by electrostatic spraying. *Prog. Org. Coat.* **2016**, *90*, 284–290. [[CrossRef](#)]
44. Park, C.; Ounaies, Z.; Watson, K.A.; Crooks, R.E.; Smith, J., Jr.; Lowther, S.E.; Connell, J.W.; Siochi, E.J.; Harrison, J.S.; St Clair, T.L. Dispersion of single wall carbon nanotubes by in situ polymerization under sonication. *Chem. Phys. Lett.* **2002**, *364*, 303–308. [[CrossRef](#)]
45. ASTM International. *ASTM Standard, B117-03, Standard Practice for Operating Salt Spray (Fog) Apparatus*; ASTM International: West Conshohocken, PA, USA, 2011. [[CrossRef](#)]
46. McCafferty, E. *Introduction to Corrosion Science*; Springer: New York, NY, USA, 2010.

47. Amirudin, A.; Thierry, D. Application of electrochemical impedance spectroscopy to study the degradation of polymer-coated metals. *Prog. Org. Coat.* **1995**, *26*, 1–28. [[CrossRef](#)]
48. Li, J.; Gan, L.; Liu, Y.; Mateti, S.; Lei, W.; Chen, Y.; Yang, J. Boron nitride nanosheets reinforced waterborne polyurethane coatings for improving corrosion resistance and antifriction properties. *Eur. Polym. J.* **2018**, *104*, 57–63. [[CrossRef](#)]
49. Potvin, E.; Brossard, L.; Larochelle, G. Corrosion protective performances of commercial low-VOC epoxy/urethane coatings on hot-rolled 1010 mild steel. *Prog. Org. Coat.* **1997**, *31*, 363–373. [[CrossRef](#)]
50. Lee, Y.L.; Luo, X.L.; Hu, S.J.; Li, Y.B.; Buchheit, R. Corrosion Protection Studies of Crude Glycerol-Based Waterborne Polyurethane Coating on Steel Substrate. *J. Electrochem. Soc.* **2016**, *163*, C54–C61. [[CrossRef](#)]
51. Hu, J.M.; Zhang, J.Q.; Cao, C.N. Determination of water uptake and diffusion of Cl⁻ ion in epoxy primer on aluminum alloys in NaCl solution by electrochemical impedance spectroscopy. *Prog. Org. Coat.* **2003**, *46*, 273–279. [[CrossRef](#)]
52. Deflorian, F.; Fedrizzi, L.; Rossi, S.; Bonora, P.L. Organic coating capacitance measurement by EIS: Ideal and actual trends. *Electrochim. Acta* **1999**, *44*, 4243–4249. [[CrossRef](#)]
53. Wong, F.; Buchheit, R.G. Utilizing the structural memory effect of layered double hydroxides for sensing water uptake in organic coatings. *Prog. Org. Coat.* **2004**, *51*, 91–102. [[CrossRef](#)]
54. Yasakau, K.A.; Carneiro, J.; Zheludkevich, M.L.; Ferreira, M.G.S. Influence of sol-gel process parameters on the protection properties of sol-gel coatings applied on AA2024. *Surf. Coat. Technol.* **2014**, *246*, 6–16. [[CrossRef](#)]
55. Ghaffari, M.S.; Naderi, R.; Sayehbani, M. The effect of mixture of mercaptobenzimidazole and zinc phosphate on the corrosion protection of epoxy/polyamide coating. *Prog. Org. Coat.* **2015**, *86*, 117–124. [[CrossRef](#)]
56. Mansfeld, F. Use of electrochemical impedance spectroscopy for the study of corrosion protection by polymer coatings. *J. Appl. Electrochem.* **1995**, *25*, 187–202. [[CrossRef](#)]
57. Funke, W. The role of adhesion in corrosion protection by organic coatings. *J. Oil Colour Chem. Assoc.* **1985**, *68*, 229–232.
58. Thomas, N.L. The barrier properties of paint coatings. *Prog. Org. Coat.* **1991**, *19*, 101–121. [[CrossRef](#)]
59. Bajat, J.B.; Milosev, I.; Jovanovic, Z.; Miskovic-Stankovic, V.B. Studies on adhesion characteristics and corrosion behaviour of vinyltriethoxysilane/epoxy coating protective system on aluminium. *Appl. Surf. Sci.* **2010**, *256*, 3508–3517. [[CrossRef](#)]
60. Lyon, S.B.; Bingham, R.; Mills, D.J. Advances in corrosion protection by organic coatings: What we know and what we would like to know. *Prog. Org. Coat.* **2017**, *102*, 2–7. [[CrossRef](#)]
61. ASTM International. *ASTM Standard, D3359, Standard Test Methods for Measuring Adhesion by Tape Test*; ASTM International: West Conshohocken, PA, USA, 2009. [[CrossRef](#)]
62. Myshkin, N.K.; Petrokovet, M.I.; Kovalev, A.V. Tribology of polymers: Adhesion, friction, wear, and mass-transfer. *Tribol. Int.* **2005**, *38*, 910–921. [[CrossRef](#)]
63. Gu, J.; Wu, G.; Zhang, Q. Effect of porosity on the damping properties of modified epoxy composites filled with fly ash. *Scr. Mater.* **2007**, *57*, 529–532. [[CrossRef](#)]
64. Suhr, J.; Koratkar, N.; Keblinski, P.; Ajayan, P. Viscoelasticity in carbon nanotube composites. *Nat. Mater.* **2005**, *4*, 134–137. [[CrossRef](#)] [[PubMed](#)]
65. Na, Y.; Cho, G. Sound absorption and viscoelastic property of acoustical automotive nonwovens and their plasma treatment. *Fibers Polym.* **2010**, *11*, 782–789. [[CrossRef](#)]
66. Qiu, M.; Zhang, Y.Z.; Bao, S.; Du, S.M.; Yan, Z.W. The relationships between tribological behaviour and heat-transfer capability of Ti6Al4V alloys. *Wear* **2007**, *263*, 653–657. [[CrossRef](#)]
67. Song, P.; Cao, Z.; Cai, Y.; Zhao, L.; Fang, Z.; Fu, S. Fabrication of exfoliated graphene-based polypropylene nanocomposites with enhanced mechanical and thermal properties. *Polymer* **2011**, *52*, 4001–4010. [[CrossRef](#)]

